Human enterovirus group B viruses rely on vimentin dynamics for efficient processing of viral non-structural proteins

Paula Turkki[1,2] Mira Laajala[1], Malin Flodström-Tullberg[3] and Varpu Marjomäki[1#]

1. Department of Biological and Environmental Science, Division of Cell and Molecular Biology / Nanoscience Center, University of Jyväskylä, Jyväskylä, Finland.
2. Faculty of Medicine and Health Technology and BioMediTech, Tampere University, Tampere, Finland,
3. Center for infectious medicine, Department of medicine Huddinge, Karolinska Institute, Karolinska University Hospital, Stockholm, Sweden

Short title: Vimentin dynamics during enterovirus infection

[#]Corresponding author:

Varpu Marjomäki

Department of Biological and Environmental Science Division of Cell and Molecular Biology / Nanoscience Center, University of Jyväskylä, Jyväskylä, Finland Phone: +358 40 5634422

E-mail: varpu.s.marjomaki@jyu.fi

ABSTRACT

We report that several viruses from the human enterovirus group B cause massive vimentin rearrangements during lytic infection. Comprehensive studies suggested that viral protein synthesis was triggering the vimentin rearrangements. Blocking the host cell vimentin dynamics with IDPN did not significantly affect the production of progeny viruses and only moderately lowered the synthesis of structural proteins such as VP1. In contrast, the synthesis of the non-structural proteins 2A, 3C, and 3D was drastically lowered. This led to attenuation of the cleavage of the host cell substrates PABP and G3BP1 and reduced caspase activation, thus leading to prolonged cell survival. Furthermore, the localization of the proteins differed in the infected cells. Capsid protein VP1 was found diffusely around the cytoplasm, whereas 2A and 3D followed vimentin distribution. Based on protein blotting, lower amounts of non-structural proteins did not result from proteasomal degradation, but from lower synthesis without intact vimentin cage structure. In contrast, inhibition of Hsp90 chaperone activity, which regulates P1 maturation, lowered the amount of VP1, but had less effect on 2A. The results suggest that, the vimentin dynamics regulate viral non-structural protein synthesis while having no effect on structural protein synthesis or overall infection efficiency. The results presented here shed new light on differential fate of structural and non-structural proteins of enteroviruses, having consequences on host cell survival.

Importance

A virus needs the host cell in order to replicate and produce new progeny viruses. For this, the virus takes over the host cell and modifies it to become a factory for viral proteins. Irrespective of the specific virus family, these proteins can be divided into structural and non-structural proteins. Structural proteins are the building blocks for the new progeny virions, whereas the non-structural proteins orchestrate the take-over of the host cell and its functions. Here we have shown a mechanism that viruses exploit in order to regulate the host cell. We show that viral protein synthesis induces vimentin cages, which promote production of specific viral proteins that eventually control apoptosis and the host cell death. This study specifies vimentin as the key regulator of these events and indicates that viral proteins have different fates in the cells depending on their association with vimentin cages.

INTRODUCTION

Human enteroviruses (EVs) are a large group of viruses including rhinoviruses, echoviruses, group A and B Coxsackieviruses, and polioviruses. They are among the most common viruses infecting humans worldwide. Most commonly, EV'-s cause acute infections, leading to lytic cell death with rapid clearance of the virus by the immune system (1). However, in some cells, infection can become persistent and lead to chronic infection (2). Deciphering the cellular events during viral infection is the key for understanding the consequences and pathology of virus infections.

Enteroviruses have four structural (VP1 to VP4) proteins that form the icosahedral virus capsid and ten non-structural (2A, 2B, 2C, 2BC, 3A, 3B, 3AB, 3C, 3D and 3CD) proteins, with several different functions. Enteroviral protease 2A cleaves the cellular eukaryotic translation initiation factor 4 G (eIF4G), poly A binding protein (PABP), controls apoptosis and induces stress granule formation (3-6). Protease 3C cleaves the cellular Ras GTPase-activating protein-binding protein 1 (G3BP1) and PABP (4, 6, 7). Protein 3D is an RNA-dependent polymerase and has been shown to be involved in the inflammatory response via the activation of NLRP3 inflammasome (8). All the viral proteins are processed from one single polyprotein and viral protein processing has been shown to be cellular chaperone mediated (9-11).

Vimentin is the most common intermediate filament in several cell types. Its expression is altered during development and in certain diseases. Vimentin has a high degree of similarity among species, suggesting that it plays a vital role in normal cellular functions. Several research groups have reported the spatial association of vimentin with viruses during

infection, particularly near the replication area and progeny virus production (12-34). Despite the abundance of such reports, there is still no consensus on the role played by vimentin during virus infections. In addition, the mechanisms by which the virus triggers vimentin remodeling remains undefined. In addition to virus infections, vimentin is associated with several significant human diseases. During cancer development, vimentin expression correlates with tumor growth, invasiveness, and poor prognosis. In addition to its structural role, vimentin has been shown to function as a key regulator of organelle positioning (35), cell migration, adhesion, and cell signaling (36).

In our earlier studies, we noticed that the morphology of the cellular vimentin network correlated with echovirus-1 (EV-1) infection efficiency in tested human cell lines (14). Changes in vimentin network brought about with different media and treatments correlated with successful baculovirus transduction and echovirus infection, suggesting that vimentin network has a previously unknown role in infection. Here we hypothesized that, in highly permissive cells, virus could modify vimentin network for its own benefits most likely via cellular stress processes that it has been shown to regulate. Here we have tested this hypothesis with careful monitoring of cellular vimentin network and several vimentin related stress responses throughout EV infection.

We show that infection by a member of the human EV group B viruses leads to massive rearrangements of the intermediate filament, vimentin. When vimentin dynamics are inhibited, expression of the viral non-structural proteins is affected, the cellular targets of 2A and 3C, PABP and G3BP1, remain uncleaved and cell death is postponed. In contrast, VP1 expression is only slightly decreased and infective progeny viruses are being produced. Our data here suggest that vimentin network plays a regulatory role in viral non-structural

protein expression, contributing to host cell survival, whereas the soluble pool of structural proteins remain largely unaffected by vimentin dynamics.

RESULTS

Human EV infection induces drastic vimentin rearrangements that start appearing by the time of replication and contain dsRNA

In order to determine the role of vimentin during EV infection, A549 cells were infected with Coxsackievirus B3 (CVB3), fixed at different time points post infection (p.i.), and immunolabeled for virus progeny capsids (VP1) and vimentin. When the composition of the vimentin network was thoroughly analyzed using confocal microscopy, it was noticed that at later stages of infection, when the cytoplasm was full of newly synthetized capsid proteins (4 to 6 h post infection (p.i.)), the majority of the infected cells showed drastic vimentin rearrangements leading to the formation of a compact vimentin cage next to the nucleus (Fig. 1A). Furthermore, tubulin labeling was done in order to ensure that the whole cytoskeleton was not affected in infected cells (Fig 1B). Cells infected with EV1, Coxsackievirus B1 (CVB1), and Coxsackie A9 virus (CVA9) showed similar vimentin rearrangements in the late stages of their lifecycle (Fig. 1C). The vimentin modifications were only seen in infected cells, indicating that these were virus-induced (Fig. 1A, C; uninfected cells shown by asterisks). Capsid protein VP1 was diffusely scattered all around the cytoplasm and on the cell edges, whereas the virus-induced vimentin structure was compact and formed in the perinuclear area (Fig. 1A, C).

We next took a look at the association between the replication intermediate dsRNA and vimentin using an antibody against double-stranded RNA (dsRNA) to mark the cells positive

for virus replication. It was noticed that vimentin formed a compartment that surrounded the dsRNA (Fig. 1D). A time course study showed that dsRNA and vimentin rearrangements both appeared around 3 to 4 h p.i. and became more pronounced during the progression of infection (Fig. 1E). Vimentin rearrangements started by first forming thicker filaments in the periphery of the cell leaving the perinuclear area, where dsRNA can usually be seen, devoid of vimentin. Then, slowly, as the signal for dsRNA increased, a thick vimentin "barrier" started to decrease in diameter and eventually, around 5 h p.i., it became a round compartment that contained dsRNA within. However, even if vimentin was accumulating in the perinuclear area, it did not drastically change the cell size or overall morphology, which was visible from the cell outlines marked in the images (Fig. 1E). As cells were still attached to the coverslips, these images verify that the vimentin structures were not formed simply due to cell rounding and detachment.

We then set out to quantify the relative amounts of cells positive for capsid protein production, to evaluate the intensity of VP1 label in the cells, to quantify the number of infected cells showing virus-induced vimentin compartments and cells positive for viral replication (dsRNA), to measure the intensity of dsRNA label in the cells, and to assess the frequency of dsRNA enwrapped by the vimentin structure during the later time points (3 to 6 h p.i.) (Fig. 2A, B). Altogether, the results showed that at 3 h p.i. around 20 percent of the cells were positive for newly-synthetized VP1 and 60 percent were positive for dsRNA. However, both the dsRNA and capsid levels per cell were still extremely low, indicating that the replication had just started. From the cells positive for progeny virus production, only 20 percent showed the typical virus-induced vimentin rearrangements at 3 h p.i. However, as the relative amount of capsids per infected cell started to increase after 4 h p.i., so did the appearance of virus-induced vimentin structures, leading to almost 80 percent of the

infected cells with vimentin compartments surrounding dsRNA. It was clear from the quantification that both dsRNA appearance and capsid protein synthesis started before the virus-induced vimentin compartments started appearing. This suggests that vimentin structure formation is not needed to initiate virus replication. Instead, the emergence of dsRNA or viral proteins could act as a trigger for the vimentin rearrangements to take place.

Vimentin dynamics are triggered by the emergence of viral proteins

We then set out to define the trigger for the virus-induced changes in vimentin distribution and structure. To determine whether virus internalization was sufficient, or whether later stages of the virus lifecycle, such as uncoating and/or replication, were needed for the virus-induced vimentin rearrangements to take place, two approaches, neutral-red viruses and UV-inactivated viruses, were used.

First, we tested neutral red-labeled CVB3-viruses (NR-CVB3), which are photosensitive and can be light inactivated resulting in uncoating-deficient viruses (Fig. 3A). Cells infected with NR-CVB3 were either kept in the dark (ctrl) or exposed to light at different time points p.i. After ten minutes of light treatment at RT, the cells were incubated at 37 °C until 5 h p.i. after which cells were fixed and immunolabeled for virus capsid and vimentin. These results showed that photo-inactivated NR-CVB3 viruses were not able to induce the vimentin rearrangements if the inactivation was performed prior to 3 h p.i., i.e. before replication had taken place. When the light inactivation was performed from 3 h p.i. onwards, virus-induced vimentin structures started appearing (Fig. 3A). Light inactivation itself did not alter vimentin network. Light-inactivation at 0 h p.i. totally prevented virus infection as determined by end-point-titration, confirming that the light inactivation was working

176 correctly (data not shown). Furthermore, NR-CVB3 kept in the dark showed high infectivity
177 (2.18 x 10^8 pfu/ml) also confirming the functionality of the NR-virus.

178 In addition to the NR-CVB3 experiment, the effect of UV-inactivated EV1 (UV-EV1) viruses
179 were tested (Fig. 3B). Cells were infected either with the wt-EV1 or with the UV-inactivated
180 EV1, fixed at 5 h p.i. and immunolabeled to visualize EV1 capsids and vimentin. As the
181 results show, UV-inactivated viruses were not able to cause the typical virus-induced
182 vimentin structures that can be seen surrounding the viral dsRNA in infected control cells.
183 These results thus suggested that mere internalization and intracellular/endosomal
184 presence of virus is not enough to trigger the vimentin changes.

185 Next, we determined whether the genome itself could act as a trigger for the vimentin
186 rearrangements or whether replication and/or protein synthesis was needed. We tested the
187 effects of cycloheximide and puromycin on cells, which have earlier been shown to inhibit
188 poliovirus protein synthesis (37). Our results showed that these treatments prevented virus-
189 induced CPE (Fig. 3C), vimentin rearrangements (Fig. 3D), and CVB3 infection as determined
190 by VP1 expression (Fig. 3E). We also confirmed an efficient inhibition of replication by
191 quantifying the (-) and (+) strand synthesis by qPCR (Fig. 3F). In order to arrest replication by
192 other means, we tested guanidine hydrochloride (GuHCl). GuHCl has been shown to inhibit
193 enteroviral 2C protein leading to inhibition of the initiation of negative strand RNA synthesis
194 (38-40). Our results showed that addition of 2 mM GuHCl in early infection completely
195 inhibited virus infection, also the protein production detected by immunolabeling of VP1
196 protein (data not shown). Subsequently, also vimentin cages did not form. Although the
197 inhibitor should not impair translation per se, it understandably has consequences on
198 silencing infection in general due to the block of replication. To further study the role of
199 replicating dsRNA, we transfected the cells with low and high concentrations of the dsRNA

analog Poly-IC and monitored vimentin dynamics. The results showed that transfection of Poly-IC into cells did not cause vimentin rearrangements (data not shown). This suggests that the cellular machinery recognizing foreign dsRNA does not trigger the events leading to vimentin dynamics during infection.

Heat shock proteins (Hsp's) and Hsp70 in particular, have been associated with several virus infections such as rabies (41) and dengue (42). Hsp90 was previously shown to be essential for the viral assembly and capsid production of Enterovirus 71 (43) and poliovirus (44) by protecting the viral components from proteasomal degradation. Also here we wanted to determine whether Hsp70 and Hsp90 had any role in vimentin dynamics during infection. To accomplish this, we used the specific inhibitor of Hsp70, VER155008, which is known to bind to the ATP-binding site of Hsp70 and to prevent substrate binding and chaperone activity. In addition, we used the Hsp90 inhibitor geldanamycin. Hsp70 and Hsp90 work in collaboration in cells so that Hsp90 receives its client proteins from hsp70 in a partially folded state. Although proteins from the Hsp family are also associated with cellular stress and survival, the inhibitors used here act only on the chaperone activity. First, we monitored the cell viability in response to VER155008 and geldanamycin. Both Hsp inhibitors were able to postpone virus-induced cell death, while VER155008 was more potent in its effect (Fig. 3G). In addition to preventing cell death, these inhibitors blocked or decreased the vimentin cage formation (Fig. 3H). This also correlated with the decrease of infectivity in total, as determined by dsRNA appearance in the infected cell cytoplasm (Fig. 3I) and VP1 expression in the cells (Fig. 3J).

Altogether, these results indicate that viral protein synthesis is dependent on functional chaperones, especially Hsp70, and that viral protein expression is essential for the vimentin structures to form.

Inhibiting vimentin dynamics delays host cell death while allowing efficient infection

Vimentin is the most common intermediate filament, but there is a shortage of drugs and treatments that can be used to modify its functions. In previous vimentin-related publications, acrylamide and calyculin A have been used to inhibit vimentin dynamics, but in our experiments with A549 cells, the recommended concentrations of these compounds led to rapid cell death (data not shown). We were also unsuccessful in completely knocking down vimentin using a siRNA approach (data not shown). Another drug that has been shown to lead to the disruption of vimentin is β, β'-Iminodipropionitrile (IDPN) (45). IDPN was found gentle enough to cause only a slight decrease in cell viability during our experimental setup in A549 cells (Fig. 4A). In addition, IDPN treatment did not induce any vimentin changes by itself (Fig. 4B). Remarkably, cells infected in the presence of IDPN were not showing signs of virus induced CPE, and cell viability remained high even 8 hp.i., whereas in control infection, already over 80 % of the infected cells had died (Fig. 4C). Strikingly, this did not correlate with progeny virus production as, indeed, IDPN treated cells efficiently produced infective virions similar to control cells as was judged by end-point titration (Fig. 4D). Also, only a slight decrease in replication was observed, based on the measurement of (+) strand synthesis using qPCR in IDPN treated cells (Fig. 4E). This was also confirmed by labeling of dsRNA (Fig. 4F). IDPN did however have a clear effect on the localization of dsRNA, as it spread out to a wider area in the cytoplasm from the perinuclear area when formation of vimentin cages was prevented with IDPN.

The location of viral non-structural proteins 3D and 2A follow the location of vimentin in the cells, whereas VP1 localization was not affected by changes in vimentin

We were then curious to monitor the expression of individual viral, both structural and non-structural proteins. Confocal microscopy of 3D polymerase showed a notable decrease in 3D expression under IDPN treatment in comparison to normal infection (Fig. 5A). In addition, the localization of the 3D signal was quite well associated with vimentin cages, whereas during IDPN treatment, the signal was spread out in the cell, similar to vimentin label. In addition to 3D, 2A protease showed a similar phenomenon (Fig. 5B). It associated more strongly with the vimentin cage during infection but spread out to all cytoplasm showing lower signal during IDPN treatment (Fig. 5B). In contrast to these results with non-structural proteins, VP1 label seemed to be similarly strong during normal infection and IDPN treatment (Fig. 5C). Also, there was no apparent shift in the location of the signal due to IDPN treatment, suggesting that the structural and non-structural proteins may be differentially located during their translation in the cytoplasm with respect to vimentin distribution. This led us to evaluate the location of other cellular components, whether their location would be sensitive to IDPN treatment. Indeed, the luminal ER marker PDI was spread out during IDPN treatment, while during infection, it was drawn to the vimentin cage area colocalizing with dsRNA (Fig. 5D). The cis-Golgi matrix protein GM130 was also found to redistribute from the typical perinuclear Golgi location towards vimentin organized cages (Fig. 5E). This process was partially prevented by IDPN treatment (Fig. 5E).

Inhibition of vimentin dynamics leads to a marked decrease in non-structural protein expression as compared to viral structural proteins

As the confocal microscopy suggested a clear difference between the expression and location of viral capsid proteins during IDPN treatment in comparison to 3D polymerase and 2A protease, we set out to quantify the amounts of VP1 and different viral non-structural

proteins. First of all, we observed that the VP1 expression was about 40 % lower than during normal infection (Fig. 6A). This was in line with the decrease seen in (+) strand synthesis (Fig. 4E). In contrast, the signals for 2A, 3C and 3D were much lower when evaluated by western blotting (Fig. 6A). Quantification of all these non-structural proteins in comparison to VP1 detected in the same blots, revealed that all signals from non-structural proteins were markedly lower than VP1, approximately only about 20 %, 10% and 1% for 2A, 3C and 3D from the amount of VP1, respectively (Fig. 6A). This decrease coincided well with the lower activity of viral proteases 2A and 3C towards some of their cellular substrates (Fig. 6B). The cellular substrate PABP and G3BP1 were left largely uncleaved despite of the infection taking place, thus leading to also higher cell viability (Fig. 6C). As these substrates have been linked to promotion of apoptosis during infection, we wanted to measure the effects of caspase activation. Indeed, the lower activity towards PABP and G3BP1 coincided with a marked decrease in caspase activation (Fig. 6D), further explaining the lack of CPE in IDPN treated infected cells.

Interestingly, the cellular substrate of 2A, the eIF4G, was rather efficiently cleaved, albeit with lower efficiency when compared to control infection (Fig. 6E). As eIF4G is linked to the host cell shutoff during viral infection, we evaluated the overall status of protein translation using metabolic labeling and observed a clear host cell shutoff both during normal infection and IDPN treatment (Fig. 6F). It thus seems that the minor effect of IDPN on eIF4G via 2A allowed still a rather efficient host cell shutoff and efficient production of viral structural proteins during IDPN treatment.

Cell killing during virus infection may also occur via ER stress. To rule out that the prolonged viability and lower cell killing during IDPN treatment had to do with ER stress response, we set out to monitor different ER stress markers and their expression (Fig. 6G). Tunicamycin

treatment (24 h) was used as a positive control. CVB3-infected cells with or without IDPN treatment did not show any similarities with tunicamycin treatment or changes in any of these marker proteins, indicating that ER stress was not induced in CVB3-mediated cell death (Fig. 6G). Reactive oxygen species (ROS) have also been associated with vimentin changes in the cells during stressful conditions. However, as we looked at the H_2O_2 induction in the cells with the aid of the ROS-Glo kit (Promega), we could only observe minor changes in CVB3 treated cells when compared to the control cells either with or without IDPN treatment (Fig. 6H).

These results altogether suggest that when vimentin dynamics are inhibited, cell killing is postponed due to low expression and activity of the non-structural viral proteases 2A and 3C and not via ER stress or ROS production.

Inhibiting vimentin dynamics slows down synthesis of especially non-structural proteins but does not accelerate degradation

According to our results, the lower amount of non-structural proteins seemed to be a key aspect mediating the prolonged viability and reduced cell killing during IDPN treatment. Our results further indicated that during IDPN treatment there is also a marked reduction in non-structural -protein expression versus structural proteins. Therefore, a crucial question to be addressed was whether the non-structural proteins are actively down-regulated or inefficiently synthetized or processed. EV polyprotein is synthetized as one unit that is then cleaved and processed into the individual structural and non-structural proteins. We first set out to define whether lower amounts of non-structural proteins is due to active degradation of those proteins. Western blot and VP1 immunostaining was performed from

samples taken at different timepoints during infection, with and without IDPN (Fig. 7A). The results showed that during normal infection the non-structural proteins 2A and 3D became visible after 4 and 5 h p.i. while VP1 was evident already earlier, starting from 3 h p.i. IDPN treatment caused lower synthesis of the VP1 and a delay in the appearance of VP1. In the same blot, 2A and 3D remained undetectable throughout the infection period. As proteasomal degradation is the main mechanism to get rid of cytoplasmic proteins, we first used the specific proteasomal inhibitor, bortezomib, to assess the levels of VP1 and 2A during viral infection with and without IDPN. The western blotting results first of all confirmed our earlier observation that VP1 was moderately down-regulated during IDPN treatment, whereas 2A was almost non-detectable after 5.5 h p.i. (Fig. 7B, blot on the right, lanes 1 and 2). Addition of bortezomib together with IDPN did not restore normal levels of VP1 or 2A, whereas they stayed similar to IDPN treatment alone, suggesting that the lower expression was not due to proteasomal degradation (Fig 7B, lanes 2, 5 and 6). This result was also confirmed with another proteasomal inhibitor lactacystin (data not shown).

We also tested the involvement of cytoplasmic neutral proteases, calpains. Calpains are ubiquitous proteases readily available in the cytoplasm and shown to be involved in promoting enterovirus infection by us and others (46-48). Addition of calpain inhibitor 1 around 2 h p.i. caused a more pronounced inhibition on VP1 than by mere IDPN treatment (Fig. 7B, lanes 2 and 3). Addition of calpain inhibitor 1 on top of IDPN treatment totally abolished viral protein production and infection (Fig. 7B, lane 4). Our recent results have shown that calpain proteases can contribute to efficient cleavage and maturation of structural proteins from the P1 region of the polyprotein (Laajala et al., unpublished). Therefore, the additive effect of calpains with IDPN to totally block both structural and non-structural proteins was expected.

342 Western blot results also confirmed that the chaperone Hsp70 inhibitor VER155008 almost
343 completely shuts down viral protein synthesis (Fig. 7B, lane 10). Hsp90 inhibitor
344 Geldanamycin, on the other hand, had almost an opposite effect for viral protein synthesis
345 in comparison to IDPN treatment: non-structural protein 2A was expressed in higher
346 amounts than in IDPN treatment, whereas VP1 was found in lower amount (Fig. 7B, lanes 2
347 and 11).

348 The results altogether confirmed that the changes in vimentin cage formation causes a
349 much higher reduction in synthesis of non-structural proteins in comparison to structural
350 proteins. The results further show that the effect is not executed via increased degradation
351 of viral proteins.

352

353

354

DISCUSSION

Several viruses have been shown to cause changes in the cellular vimentin network during infection. There are several postulations on the role of vimentin dynamics, but no consensus has been found so far for the mechanisms of action. Vimentin aggregating or collapsing to make a perinuclear compartment has been previously reported with the closely related viruses enterovirus 71 and Foot- and-mouth disease virus (20), but also for less closely related viruses such as vaccinia virus (18), iridovirus (25), bluetongue virus (23), parvovirus (30, 31), African swine fever virus (34), Epstein-Bar virus (19), and dengue virus (16, 29, 32, 49, 50). These aggregates have been shown to surround the replicating DNA (18), dsRNA (16), non-structural or newly synthetized structural proteins (16, 20, 23, 29, 32), leading the authors to suggest that vimentin acts to surround the replication and assembly sites and to have a scaffolding or a protective role. Similarly, in our studies, the hallmark of these virus-induced vimentin structures was the cage formation to surround the replication intermediate dsRNA. However, as vimentin rearrangements also led to ER and Golgi rearrangements, it could be postulated that the dsRNA was concentrating inside these vimentin structures by the redistribution of the ER and Golgi, which provides membranes for the replication processes. In fact, when the formation of these vimentin structures was inhibited, replication and progeny virus production continued, but dsRNA, NS-proteins and ER were more diffusely located around the cell. Translocation of the ER has been previously reported also for dengue virus infection (16). Although the presence of dsRNA or other replication elements within these structures was a constant feature in previously published studies, our results here show that the clustering of replication-associated structures inside the vimentin cage is not a necessary factor for infection and production for progeny viruses.

Our studies show that the formation of vimentin structures was dependent on viral protein translation based on several lines of evidence: 1) Cage formation was inhibited when either UV-inactivated or light-inactivated (neutral red treated) replication-incompetent viruses were used. 2) The structures were not seen when cells were transfected with a dsRNA analog or when infected cells were treated with protein synthesis inhibitors. Finally, 3) the appearance of the structures coincided with the time of viral protein synthesis and could be inhibited by perturbing the function of Hsp70, which efficiently blocked viral protein synthesis (9). Taking this into consideration, we were surprised to see that none of the ER stress markers were upregulated during infection.

Vimentin has been previously shown to protect Hepatitis C virus core protein and the cellular protein Scrib from host mediated proteasomal degradation (15) (51). Proteasomal degradation of hepatitis C virus core protein was inhibited by MG-132, an inhibitor of proteasomal and calpain degradation. In our experiments MG-132 efficiently inhibited virus infection (data not shown) because of the strong dependence of enterovirus infection on calpain proteases ((48), Laajala et al, unpublished). MG-132 is a strong inhibitor of calpains and therefore, in our study, more specific inhibitors of proteasomal degradation was used, e.g. bortezomib and lactacystin. Those studies showed clearly that proteasomal degradation was not involved in IDPN induced effects.

In addition to rapid life cycle and clear cytopathic effect, also the ability to cease host cell protein synthesis is a hallmark of enterovirus infection. Enteroviral host cell shut off and the onset of host cell apoptosis have been linked to the actions of the viral proteases 2A and 3C. Enteroviruses commonly have three viral proteases, which are in charge of viral polyprotein processing and cleavage of cellular targets (52). Protease 3CD is involved in the cleavage of P1 leading to the maturation of the capsid proteins VP1, VP2 and VP0. Pro 2A is believed to

autocatalytically cleave P1 from P2 while 3C and 3CD are supposed to take care of other polyprotein cleavages. In our results, we could observe low amounts of 3D, 3C and 2A expression with IDPN treatment by immunoblotting and immunofluorescence staining. Still, VP1 was observed in rather high amounts and, surprisingly, normal amounts of infectious particles were generated during IDPN treatment. We have unpublished information that calpain proteases 1 and 2 are able to correctly cleave capsid proteins from P1 (Laajala et al. unpublished). Thus, the ubiquitously present calpain proteases in the cytoplasm could contribute to capsid protein processing and explain the almost normal amounts of VP1 during IDPN treatment with lower 3C and 3CD expression. It seems that the low amount of 2A observed during IDPN treatment is enough to efficiently execute the cleavage of P1 out of P2-P3. Also, low amount of 3D polymerase was observed, which clearly produced enough RNA for the assembly of infectious viral particles.

The cellular targets of 2A and 3C, PABP and G3BP1 are partially responsible for the host cell shut-off. Therefore, it was a surprise that, despite of their low amounts, virus infection was accompanied by a rather efficient host-cell-shutoff. From the cellular targets, the eIF4G cleavage was the least affected, and thus perhaps being responsible for the strong reduction of host cell protein production. During IDPN treatment, ample RNA and structural proteins were still produced during the first 6 hours of infection. Still, the high virus yields was somewhat unexpected because of the detected lower amounts of non-structural proteins. It is however likely that at later time points the virus yields are bound to get lower. Rather than affecting the virus yields or host-cell-shutoff, the more important consequence of the lowered synthesis of the 2A and 3C/3CD was the reduced caspase activation. Caspase 3/7 activation was clearly compromised leading to higher viability, while the viral protein and RNA production continued almost in a normal pace.

Our findings show that human enterovirus infection leads to massive vimentin rearrangements that harbor the replication site, as was indicated by the higher association of dsRNA, 2A and 3D polymerase with the vimentin cages. Many RNA viruses, including enteroviruses, have been shown to cause massive membrane rearrangements in the host cell during replication. The formation of these replication organelles have been shown to be caused by the viral non-structural proteins such as 3A (53). The replication organelles appear first as single membrane tubular structures, which evolve into double-membrane vesicles, which serve as platforms for replication (54, 55). Since both the time of appearance and localization into perinuclear area coincides for replication organelles and vimentin cage (54, 55), vimentin is likely to have a role in the formation or support of the replication area. In addition, when the vimentin dynamics were prevented, the replication area was more spread out, further suggesting that vimentin contributes to the organization of the replication area. Moreover, it can be speculated that the sequestration of replication area into vimentin cage may protect the virus from e.g. pattern recognition receptors (PRRs) of the host. These PRRs are part of the innate immune system and protect the host from pathogens by recognizing foreign molecules such as dsRNA (56). However, whether vimentin cage protects enteroviruses against innate immune response of the host cell, remains to be shown.

Importantly, we also observed that the replication sites did not particularly accumulate structural proteins such as VP1, which was widely distributed around the cell and was thus less affected by the IDPN treatment. Instead, the inhibition of these structures reduced the synthesis levels of 2A, 3C and 3D and processing rather than their selective degradation. The results thus indicated that, due to IDPN treatment, cleavage products of P1 and P2 (VP1 and 2A, respectively) were produced in different ratios. It has been shown that the processing of

P1 out from the polyprotein occurs co-translationally, when 2A rapidly cleaves between itself and VP1 as soon as the required components have been translated (57, 58). In the light of our results, perhaps the synthesis of the rest of the polyprotein (P2-P3) is then dependent on vimentin dynamics and takes place efficiently only if vimentin is specifically arranged. However, it will be important to study the true mechanistic basis behind these phenomena in the future. Speculatively, one explanation could be the various non-canonical translation pathways that RNA viruses use to translate multitude of proteins from their compact mRNA (59). Many RNA-viruses use non-canonical translation such as ribosomal frameshifting in order to regulate the ratios of different viral proteins, most commonly allowing greater production of structural proteins (60, 61), among those also cardiovirus and FMDV from the picornavirus family (62, 63). Whether such mechanisms are contributing to the observed different ratios of non-structural and structural protein synthesis and processing for CVB3 as well remains to be shown.

Interestingly, Hsp90 inhibitor geldanamycin caused an arrest in VP1 production, while the effect in non-structural proteins was much milder. Hsp90 is known to bind P1 and contribute to P1 processing (11, 44). Thus, results with Hsp90 also suggest that different cellular mechanisms may affect P1 and production of structural proteins in contrast to non-structural proteins. Vimentin has been shown to co-immunoprecipitate 2C of the foot-and-mouth disease virus, and they together organize replication sites for efficient infection (20). Influenza A virus viral ribonucleoprotein was also shown to be bound by vimentin in the cytoplasm and thus preventing it from entering the nucleus and rather downregulating the infection (64). Interestingly, Lawson and Semler (65) showed using metabolic labeling of poliovirus 1 that much of the P1 and structural proteins accumulate in the cytosolic soluble fraction although P1 also stays partially membrane bound. In contrast, most of the non-

structural proteins as well as P2 and P3 associate with the membrane bound fraction, supposedly the replication structures. Their results suggested that P2 and P3 processing is active early in infection in vivo in the membranous fraction, but does not occur anymore when P2, 3CD and P3 later appear in the soluble fraction. In contrast, P1 is actively processed further in the soluble fraction for longer periods. These results suggest that the distribution of P2-P3 and their individual proteins in soluble cytosolic or membrane bound fraction largely determines their activity in polyprotein processing (Fig. 8). It seems likely that vimentin cage organizes the replication structures together with 2C and provides an optimal niche for the initial replication/translation to occur and to produce viral proteases 2A, 3C and 3CD as well as 3D polymerase. Without the cage formation, the replication area is less organized, and the synthesis of non-structural proteins is less efficient while VP1 production occurs almost normally in the soluble fraction. However, it will be important to study in the future, which factors exactly trigger vimentin rearrangements and also reveal the molecular mechanism behind the cage formation. Although we showed the effect of vimentin rearrangements specifically during the infection of enterovirus B species, it is likely that also other enterovirus species (A, C, D) would show similar dependence on vimentin rearrangements, taking into account the similarity of replication process among different species.

In conclusion, we show that viral protein synthesis during enterovirus infection induces formation of a vimentin enwrapped perinuclear compartment harboring replicating dsRNA and non-structural proteins 3D and 2A. In turn, inhibition of vimentin rearrangements leads to scattered distribution of non-structural proteins and their lower expression and activity. This leads to delayed onset of apoptosis and higher viability of the host cells. In contrast, location and expression level of structural proteins such as VP1 stays largely unchanged, promoting efficient virus production. Altogether these results show that vimentin dynamics,

taking place in the infected cells, regulate the non-structural protein synthesis, without compromising infection efficiency but affecting host cell survival.

503 **MATERIALS AND METHODS**

504

505 **Cells.** Human alveolar basal epithelial cell line A549 and human cervix adenocarcinoma cell
506 line HeLa MZ we used for the experiments. The cell lines were obtained from American type
507 cell culture (ATCC) and grown in humidified 5% (v/v) CO2 at 37°C in Dulbecco's modified
508 Eagle's medium (DMEM, Invitrogen) supplemented with 5% to 10% fetal bovine serum (FBS)
509 supplemented with Glutamax (Invitrogen) and penicillin and streptomycin (P/S).

510 **Viruses.** EV1 (Farouk strain), CVA9 (Griggs strain), CVB1 (Conn5 strain) and CVB3 (Nancy
511 strain) were obtained from ATCC and propagated in green monkey kidney (GMK) cells. The
512 virus was released from infected GMKs by freeze-thawing and concentrated by
513 centrifugation into a sucrose cushion. Infectivity of the produced virus stock was assayed
514 with an endpoint titration and viruses were used in excess in order to quarantee efficient
515 infection (MOI 65) in A549 cells. When ice binding was used, the pfu/ml is mentioned for
516 each experiment. For all infection studies, the culture medium was supplemented with 1 to
517 5 % FBS.

518 **End point dilution.** The assay was carried out in GMK cells (ATCC) cultured in 96-well plate.
519 Cells were infected with CVB3 by preparing a dilution series in MEM supplemented with 1%
520 FBS and 1% GlutaMAX. After 3 days of infection at + 37 °C, the cells were stained for 10 min
521 with 50 µl of crystal violet stain (8.3 mM crystal violet, 45 mM CaCl2, 10% ethanol, 18.5%
522 formalin, and 35 mM Tris base). The excess stain was washed with water, and the infectivity
523 was determined based on the number of dyed (non-infected) and non-dyed (infected) wells.
524 The 50% tissue culture infective dose (TCID50) was calculated by comparing the number of
525 infected and uninfected wells for eight replicates of the same virus concentration. The
526 concentration at which half of the wells would be infected was extrapolated (TCID50).

Finally, the TCID50 value was multiplied by 0.7 to obtain the PFU/ml value. End-point dilution for NR-CVB3 was done after inactivating the virus with light for 10 min or keeping the virus in the dark as a control.

Reagents. Cycloheximide, Puromycin, tunicamycin and VER-155008 were purchased from Sigma-Aldricht whereas caspase inhibitor Z-VAD-fmk, caspase glo 3/7 assay –kit, ROS activity and cell titer glo- cell viability kit were obtained from Promega. Other reagents included Annexin V (Abcam), IDPN (Alfa Aesar), staurosporin (Enzo), Calpain inhibitor I (Roche), Geldanamycin (Enzo), Bortezomib (LC laboratories) and GuHCl (Sigma).

Immunolabeling. In all immunofluorescence and confocal microscopy studies, the cells were grown on coverslips and fixed with 3 to 4 % PFA-PBS. Permeabilization, when needed, was performed with 0.1-0.2% Triton X-100-PBS. All used antibodies were diluted in 3% BSA-PBS and cells were stained by using a standard protocol for immunofluorescence staining with appropriate antibodies. Fluorescent conjugated goat secondary antibodies against mouse or rabbit antibodies were from Life Technologies. The coverslips were mounted with ProLong Gold Antifade Reagent with DAPI (life technologies).

SDS-PAGE and western blotting. Cell lysates were suspended in laemmli buffer containing mercaptoethanol. Samples were separated in 12 % SDS-polyacrylamide gel or in 4-20% miniprotean TGX stain free gel (Biorad) and electroblotted into polyvinylidene difluoride membrane (Millipore). Appropriate primary antibodies together with horseradish peroxidase conjugated secondary antibodies were used in immunoblotting. Bands were detected by supersignal chemiluminescence detection kit (Thermo Scientific) and developed into X-ray film or imaged with Chemidoc MP (Biorad).

Antibodies. To detect CVA9, CVB1 and CVB3 either polyclonal rabbit antiserum against CVA and CVB (kindly provided by Roivainen et al) or monoclonal antibody against EVs (ncl-

551 entero, clone 5-D8/1) (Novocastra) was used. For detection of EV1, rabbit antisera against
552 purified EV1 (66) was used. Antibodies against the ER-stress markers were obtained from
553 ER-stress antibody sampler kit (cell signaling technologies). Other antibodies were
554 monoclonal (NCL-VIM-V9, Leica microsystems) and rabbit polyclonal antibody against
555 vimentin (H-84) (Santa Cruz biotechnology Inc.) in addition to monoclonal antibody against
556 dsRNA (J2, English & Scientific Consulting Kft). GM130 and PDI antibodies were from Abcam
557 and G3BP1, PABP, eIF4G and GAPDH antibodies were from Santa Cruz. Antibody against
558 beta-tubulin was from Cedarlane. Viral protease antibodies have been previously published
559 (67). Antibody against 3D was a kind gift from Antonio Toniolo, (Università dell'Insubria,
560 Italy).

561 **Transfection of Poly-IC.** A549 cells were transfected with Poly-IC (Santa Cruz) using
562 Lipofectamine 3000. The amount of Poly-IC was 1 ng/µl or 50 ng/µl and transfection was
563 carried out according to the instructions by the manufacturer. Cells were fixed with 4% PFA
564 after 2, 4 or 6 h post-transfection. As control, cells were treated with transfection reagents
565 only with no poly-IC.

566 **RT-qPCR.** CVB3 infected A549 cells were freeze-thawed three times and cell debris pelleted
567 down at full speed with table top centrifuge. Viral RNA from the supernatant was extracted
568 according to the instructions of the manufacturer using QiAmp viral RNA Mini Kit (Qiagen).
569 Reverse transcription was carried out for positive or negative strand RNA using either 1.2
570 µM antisense (5'-GAAACACGGACACCCAAAGTA) or sense (5'-CGGCCCCTGAATGCGGCTAA)
571 primers, 20 U M-MLV reverse transcriptase (Promega), 4 U RNAsin ribonuclease inhibitor
572 (Promega) and dNTPs (Promega). From the reverse transcription reaction mixture (40 µl), 5
573 µl was taken for PCR reaction, which also contained Sybr green supermix (Biorad) and 600
574 nM of each primers. PCR was performed using C1000 Touch Thermal cycler (CFX96 real-time

system; Biorad) and the amplification steps were as follows: 95°C for 10 min; 40 cycles of 95°C for 15 s to 60 °C for 1 min and final melt at 72 to 95°C, 1°C/5 s. The assay contained three replicates of each sample and also contained negative controls to confirm the specificity of the products.

Metabolic labeling. A549 cells were infected with 4.43 x 10^8 PFU/ml of CVB3. The virus was bound on ice for 1 h, after which the excess virus was washed with PBS. 1.5% IDPN in DMEM supplemented with 1% FBS was added after ice binding. After addition of IDPN, it was present at all steps until the end of the experiment. The infection was allowed to proceed in + 37 ºC for 4 h, after which the low methionine/cysteine medium supplemented with dialyzed 1% FBS was added on cells. After 30 min, 500 µCi/ml of [^{35}S] methionine-cysteine was added before a 1 h pulse. Samples were run at 4-20% miniprotean TGX stain free gel (Biorad), after which the gel was fixed with 30% methanol, 10% acetic acid for 30 min. Next, the gel was treated with an autoradiography enhancer (Enlightning; PerkinElmer) for 30 min. Finally, the gel was dried at +70°C for 2 h (Gel dryer 583; Bio-Rad) and the dried gel was subjected to autoradiography.

UV-inactivated EV1. Previous experiments for UV inactivation of picornaviruses (68, 69) were used as a guide for the general settings. Viruses were irradiated with Sylvania UV-C lamp (Ultraviolet 8H, 630W, Japan) with the intensity of 1.8 mW/cm2 for 30s. Lamp intensity was calibrated with spectrophotometer.

Neutral red CVB3. NR-CVB3 were produced in the presence of 10 µg/ml of NR (catalog number 101369; Merck). The virus was released after overnight infection by freeze-thawing the cells and harvested by centrifugation. During the experiment, cells were kept in dark except for light inactivation which was for 10 minutes.

598 **Crystal violet experiment (CPE).** The cells were washed with PBS to remove the detached
599 cell. Remaining cells were stained with crystal violet stain (0.03 % wt/vol crystal violet; 2 %
600 ethanol; 3 % formalin in water). The plate was incubated at RT for 10 min and the unbound
601 stain removed. After washes with sterile water, lysis buffer (8.98 % wt/vol sodium citrate,
602 125 mM HCl, 47.0 % EtOH) was added to the cells and absorbance was measured from the
603 homogenized solution at wavelength 570 nm using Victor microplate reader.

604 **Imaging and analysis.** Samples were imaged with Olympus FV1000-IX81 or Zeiss LSM700
605 confocal microscopes. Appropriate excitation and emission settings were used (405-nm
606 diode laser, 488-nm argon laser and 543-nm HeNe-laser). 60x UPLSAPO objective (NA 1.35)
607 and 20x/0.5 EC Plan-Neofluar objective with resolution of 512×512 or 640x640 pixels/image
608 were used. Levels for the laser power, detector amplification, and optical sections were
609 optimized for each channel before starting the imaging. The threshold for each channel was
610 adjusted to separate the signal from noise and data from the images was quantified using a
611 free, open source software package, BioImageXD (70). In order to quantitate the relative
612 amount of antigen per cell, the total intensity was divided with DAPI-stained nucleus volume
613 or with the total intensity of another antigen to gain the ratio of different antigens. For
614 quantification of fluorescent intensities and the relative amount of the immunolabeled
615 antigen, at least 30 cells from three independent experiments were imaged unless
616 otherwise stated. Quantification were done on single-section images taken from the center
617 of the cell.

618 **Statistical analysis.** Statistical analysis was performed with GraphPad Prism software.
619 Statistical significance of pair wise differences was determined by student´s t-test. All data
620 is presented as mean ± SEM.

621

622

623 **REFERENCES**

624

625 1. **Harris, K. G., and C. B. Coyne.** 2014. Death waits for no man--does it wait for a virus? How
626 enteroviruses induce and control cell death. Cytokine Growth Factor Rev. **25:**587-596. doi:
627 10.1016/j.cytogfr.2014.08.002 [doi].

628 2. **Alidjinou, E. K., F. Sane, I. Engelmann, V. Geenen, and D. Hober.** 2014. Enterovirus
629 persistence as a mechanism in the pathogenesis of type 1 diabetes. Discov. Med. **18:**273-
630 282.

631 3. **Kuo, R. L., S. H. Kung, Y. Y. Hsu, and W. T. Liu.** 2002. Infection with enterovirus 71 or
632 expression of its 2A protease induces apoptotic cell death. J. Gen. Virol. **83:**1367-1376. doi:
633 10.1099/0022-1317-83-6-1367 [doi].

634 4. **Rivera, C. I., and R. E. Lloyd.** 2008. Modulation of enteroviral proteinase cleavage of
635 poly(A)-binding protein (PABP) by conformation and PABP-associated factors. Virology.
636 **375:**59-72. doi: 10.1016/j.virol.2008.02.002 [doi].

637 5. **Chau, D. H., J. Yuan, H. Zhang, P. Cheung, T. Lim, Z. Liu, A. Sall, and D. Yang.** 2007.
638 Coxsackievirus B3 proteases 2A and 3C induce apoptotic cell death through mitochondrial
639 injury and cleavage of eIF4GI but not DAP5/p97/NAT1. Apoptosis. **12:**513-524. doi:
640 10.1007/s10495-006-0013-0 [doi].

641 6. **Dougherty, J. D., W. C. Tsai, and R. E. Lloyd.** 2015. Multiple Poliovirus Proteins Repress
642 Cytoplasmic RNA Granules. Viruses. **7:**6127-6140. doi: 10.3390/v7122922 [doi].

643 7. **White, J. P., A. M. Cardenas, W. E. Marissen, and R. E. Lloyd.** 2007. Inhibition of
644 cytoplasmic mRNA stress granule formation by a viral proteinase. Cell. Host Microbe. **2:**295-
645 305. doi: S1931-3128(07)00222-3 [pii].

646 8. **Wang, W., F. Xiao, P. Wan, P. Pan, Y. Zhang, F. Liu, K. Wu, Y. Liu, and J. Wu.** 2017. EV71
647 3D Protein Binds with NLRP3 and Enhances the Assembly of Inflammasome Complex. PLoS
648 Pathog. **13:**e1006123. doi: 10.1371/journal.ppat.1006123 [doi].

649 9. **Mayer, M. P.** 2005. Recruitment of Hsp70 chaperones: a crucial part of viral survival
650 strategies. Rev. Physiol. Biochem. Pharmacol. **153:**1-46. doi: 10.1007/s10254-004-0025-5
651 [doi].

652 10. **Wang, R. Y., R. L. Kuo, W. C. Ma, H. I. Huang, J. S. Yu, S. M. Yen, C. R. Huang, and S. R.**
653 **Shih.** 2013. Heat shock protein-90-beta facilitates enterovirus 71 viral particles assembly.
654 Virology. **443:**236-247. doi: 10.1016/j.virol.2013.05.001 [doi].

655 11. **Newman, J., A. S. Asfor, S. Berryman, T. Jackson, S. Curry, and T. J. Tuthill.** 2018. The
656 Cellular Chaperone Heat Shock Protein 90 Is Required for Foot-and-Mouth Disease Virus
657 Capsid Precursor Processing and Assembly of Capsid Pentamers. J. Virol.
658 **92:**10.1128/JVI.01415-17. Print 2018 Mar 1. doi: e01415-17 [pii].

659 12. **Liebowitz, D., R. Kopan, E. Fuchs, J. Sample, and E. Kieff.** 1987. An Epstein-Barr virus
660 transforming protein associates with vimentin in lymphocytes. Mol. Cell. Biol. **7:**2299-2308.

661 13. **Ghosh, S., W. A. Ahrens, S. U. Phatak, S. Hwang, L. W. Schrum, and H. L. Bonkovsky.**
662 2011. Association of filamin A and vimentin with hepatitis C virus proteins in infected human
663 hepatocytes. J. Viral Hepat. **18:**e568-77. doi: 10.1111/j.1365-2893.2011.01487.x;
664 10.1111/j.1365-2893.2011.01487.x.

665 14. **Turkki, P., K. E. Makkonen, M. Huttunen, J. P. Laakkonen, S. Yla-Herttuala, K. J.**
666 **Airenne, and V. Marjomaki.** 2013. Cell susceptibility to baculovirus transduction and
667 echovirus infection is modified by PKC phosphorylation and vimentin organization. J. Virol. .
668 doi: 10.1128/JVI.01004-13.

669 15. **Nitahara-Kasahara, Y., M. Fukasawa, F. Shinkai-Ouchi, S. Sato, T. Suzuki, K. Murakami,**
670 **T. Wakita, K. Hanada, T. Miyamura, and M. Nishijima.** 2009. Cellular vimentin content
671 regulates the protein level of hepatitis C virus core protein and the hepatitis C virus
672 production in cultured cells. Virology. **383:**319-327. doi: 10.1016/j.virol.2008.10.009 [doi].

673 16. **Teo, C. S., and J. J. Chu.** 2014. Cellular vimentin regulates construction of dengue virus
674 replication complexes through interaction with NS4A protein. J. Virol. **88:**1897-1913. doi:
675 10.1128/JVI.01249-13 [doi].

676 17. **Mahonen, A. J., K. E. Makkonen, J. P. Laakkonen, T. O. Ihalainen, S. P. Kukkonen, M. U.**
677 **Kaikkonen, M. Vihinen-Ranta, S. Yla-Herttuala, and K. J. Airenne.** 2010. Culture medium
678 induced vimentin reorganization associates with enhanced baculovirus-mediated gene
679 delivery. J. Biotechnol. **145:**111-119. doi: 10.1016/j.jbiotec.2009.11.003.

680 18. **Risco, C., J. R. Rodriguez, C. Lopez-Iglesias, J. L. Carrascosa, M. Esteban, and D.**
681 **Rodriguez.** 2002. Endoplasmic reticulum-Golgi intermediate compartment membranes and
682 vimentin filaments participate in vaccinia virus assembly. J. Virol. **76:**1839-1855.

683 19. **Meckes, D. G.,Jr, N. F. Menaker, and N. Raab-Traub.** 2013. Epstein-Barr virus LMP1
684 modulates lipid raft microdomains and the vimentin cytoskeleton for signal transduction
685 and transformation. J. Virol. **87:**1301-1311. doi: 10.1128/JVI.02519-12 [doi].

686 20. **Gladue, D. P., V. O'Donnell, R. Baker-Branstetter, L. G. Holinka, J. M. Pacheco, I. F.**
687 **Sainz, Z. Lu, X. Ambroggio, L. Rodriguez, and M. V. Borca.** 2013. Foot-and-mouth disease
688 virus modulates cellular vimentin for virus survival. J. Virol. . doi: 10.1128/JVI.00448-13.

689 21. **Zhang, X., H. Shi, J. Chen, D. Shi, H. Dong, and L. Feng.** 2015. Identification of the
690 interaction between vimentin and nucleocapsid protein of transmissible gastroenteritis
691 virus. Virus Res. **200:**56-63. doi: 10.1016/j.virusres.2014.12.013 [doi].

692 22. **Banerjee, I., Y. Miyake, S. P. Nobs, C. Schneider, P. Horvath, M. Kopf, P. Matthias, A.**
693 **Helenius, and Y. Yamauchi.** 2014. Influenza A virus uses the aggresome processing
694 machinery for host cell entry. Science. **346:**473-477. doi: 10.1126/science.1257037 [doi].

695 23. **Bhattacharya, B., R. J. Noad, and P. Roy.** 2007. Interaction between Bluetongue virus
696 outer capsid protein VP2 and vimentin is necessary for virus egress. Virol. J. **4:**7. doi:
697 10.1186/1743-422X-4-7.

698 24. **Plummer, E. M., D. Thomas, G. Destito, L. P. Shriver, and M. Manchester.** 2012.
699 Interaction of cowpea mosaic virus nanoparticles with surface vimentin and inflammatory
700 cells in atherosclerotic lesions. Nanomedicine (Lond). **7:**877-888. doi: 10.2217/nnm.11.185;
701 10.2217/nnm.11.185.

702 25. **Chen, M., R. Goorha, and K. G. Murti.** 1986. Interaction of frog virus 3 with the
703 cytomatrix. IV. Phosphorylation of vimentin precedes the reorganization of intermediate
704 filaments around the virus assembly sites. J. Gen. Virol. **67 (Pt 5):**915-922.

705 26. **Das, S., V. Ravi, and A. Desai.** 2011. Japanese encephalitis virus interacts with vimentin
706 to facilitate its entry into porcine kidney cell line. Virus Res. **160:**404-408. doi:
707 10.1016/j.virusres.2011.06.001.

708 27. **Miller, M. S., and L. Hertel.** 2009. Onset of human cytomegalovirus replication in
709 fibroblasts requires the presence of an intact vimentin cytoskeleton. J. Virol. **83:**7015-7028.
710 doi: 10.1128/JVI.00398-09.

711 28. **Belin, M. T., and P. Boulanger.** 1987. Processing of vimentin occurs during the early
712 stages of adenovirus infection. J. Virol. **61:**2559-2566.

713 29. **Lei, S., Y. P. Tian, W. D. Xiao, S. Li, X. C. Rao, J. L. Zhang, J. Yang, X. M. Hu, and W. Chen.**
714 2013. ROCK is involved in vimentin phosphorylation and rearrangement induced by dengue
715 virus. Cell Biochem. Biophys. **67:**1333-1342. doi: 10.1007/s12013-013-9665-x [doi].

716 30. **Nuesch, J. P., S. Lachmann, and J. Rommelaere.** 2005. Selective alterations of the host
717 cell architecture upon infection with parvovirus minute virus of mice. Virology. **331:**159-174.
718 doi: 10.1016/j.virol.2004.10.019.

719 31. **Fay, N., and N. Pante.** 2013. The intermediate filament network protein, vimentin, is
720 required for parvoviral infection. Virology. **444:**181-190. doi: 10.1016/j.virol.2013.06.009
721 [doi].

722 32. **Kanlaya, R., S. N. Pattanakitsakul, S. Sinchaikul, S. T. Chen, and V. Thongboonkerd.**
723 2010. Vimentin interacts with heterogeneous nuclear ribonucleoproteins and dengue
724 nonstructural protein 1 and is important for viral replication and release. Mol. Biosyst.
725 **6:**795-806. doi: 10.1039/b923864f.

726 33. **Khakhulina, T. V., G. K. Vorkunova, E. E. Manukhina, and A. G. Bukrinskaia.** 1999.
727 Vimentin intermediate filaments are involved in replication of human immunodeficiency
728 virus type I. Dokl. Akad. Nauk. **368:**706-708.

729 34. **Stefanovic, S., M. Windsor, K. I. Nagata, M. Inagaki, and T. Wileman.** 2005. Vimentin
730 rearrangement during African swine fever virus infection involves retrograde transport
731 along microtubules and phosphorylation of vimentin by calcium calmodulin kinase II. J. Virol.
732 **79:**11766-11775. doi: 10.1128/JVI.79.18.11766-11775.2005.

733 35. **Styers, M. L., G. Salazar, R. Love, A. A. Peden, A. P. Kowalczyk, and V. Faundez.** 2004.
734 The endo-lysosomal sorting machinery interacts with the intermediate filament
735 cytoskeleton. Mol. Biol. Cell. **15:**5369-5382. doi: 10.1091/mbc.E04-03-0272 [doi].

736 36. **Ivaska, J., H. M. Pallari, J. Nevo, and J. E. Eriksson.** 2007. Novel functions of vimentin in
737 cell adhesion, migration, and signaling. Exp. Cell Res. **313:**2050-2062. doi:
738 10.1016/j.yexcr.2007.03.040.

739 37. **Barton, D. J., B. J. Morasco, and J. B. Flanegan.** 1999. Translating ribosomes inhibit
740 poliovirus negative-strand RNA synthesis. J. Virol. **73:**10104-10112.

741 38. **Barton, D. J., and J. B. Flanegan.** 1997. Synchronous replication of poliovirus RNA:
742 initiation of negative-strand RNA synthesis requires the guanidine-inhibited activity of
743 protein 2C. J. Virol. **71:**8482-8489.

744 39. **Pfister, T., and E. Wimmer.** 1999. Characterization of the nucleoside triphosphatase
745 activity of poliovirus protein 2C reveals a mechanism by which guanidine inhibits poliovirus
746 replication. J. Biol. Chem. **274:**6992-7001. doi: 10.1074/jbc.274.11.6992 [doi].

747 40. **Banerjee, R., M. K. Weidman, A. Echeverri, P. Kundu, and A. Dasgupta.** 2004.
748 Regulation of poliovirus 3C protease by the 2C polypeptide. J. Virol. **78:**9243-9256. doi:
749 10.1128/JVI.78.17.9243-9256.2004 [doi].

750 41. **Lahaye, X., A. Vidy, B. Fouquet, and D. Blondel.** 2012. Hsp70 protein positively regulates
751 rabies virus infection. J. Virol. **86:**4743-4751. doi: 10.1128/JVI.06501-11 [doi].

752 42. **Taguwa, S., K. Maringer, X. Li, D. Bernal-Rubio, J. N. Rauch, J. E. Gestwicki, R. Andino,**
753 **A. Fernandez-Sesma, and J. Frydman.** 2015. Defining Hsp70 Subnetworks in Dengue Virus
754 Replication Reveals Key Vulnerability in Flavivirus Infection. Cell. **163:**1108-1123. doi:
755 10.1016/j.cell.2015.10.046 [doi].

756 43. **Tsou, Y. L., Y. W. Lin, H. W. Chang, H. Y. Lin, H. Y. Shao, S. L. Yu, C. C. Liu, E. Chitra, C.**
757 **Sia, and Y. H. Chow.** 2013. Heat shock protein 90: role in enterovirus 71 entry and assembly
758 and potential target for therapy. PLoS One. **8:**e77133. doi: 10.1371/journal.pone.0077133
759 [doi].

760 44. **Geller, R., M. Vignuzzi, R. Andino, and J. Frydman.** 2007. Evolutionary constraints on
761 chaperone-mediated folding provide an antiviral approach refractory to development of
762 drug resistance. Genes Dev. **21:**195-205. doi: 21/2/195 [pii].

763 45. **Galigniana, M. D., J. L. Scruggs, J. Herrington, M. J. Welsh, C. Carter-Su, P. R. Housley,**
764 **and W. B. Pratt.** 1998. Heat shock protein 90-dependent (geldanamycin-inhibited)
765 movement of the glucocorticoid receptor through the cytoplasm to the nucleus requires
766 intact cytoskeleton. Mol. Endocrinol. **12:**1903-1913. doi: 10.1210/mend.12.12.0204 [doi].

767 46. **Bozym, R. A., K. Patel, C. White, K. H. Cheung, J. M. Bergelson, S. A. Morosky, and C. B.**
768 **Coyne.** 2011. Calcium signals and calpain-dependent necrosis are essential for release of
769 coxsackievirus B from polarized intestinal epithelial cells. Mol. Biol. Cell. **22:**3010-3021. doi:
770 10.1091/mbc.E11-02-0094 [doi].

771 47. **Bozym, R. A., S. A. Morosky, K. S. Kim, S. Cherry, and C. B. Coyne.** 2010. Release of
772 intracellular calcium stores facilitates coxsackievirus entry into polarized endothelial cells.
773 PLoS Pathog. **6:**e1001135. doi: 10.1371/journal.ppat.1001135 [doi].

774 48. **Upla, P., V. Marjomaki, L. Nissinen, C. Nylund, M. Waris, T. Hyypia, and J. Heino.** 2008.
775 Calpain 1 and 2 are required for RNA replication of echovirus 1. J. Virol. **82:**1581-1590.

776 49. **Chen, Y., T. Maguire, R. E. Hileman, J. R. Fromm, J. D. Esko, R. J. Linhardt, and R. M.**
777 **Marks.** 1997. Dengue virus infectivity depends on envelope protein binding to target cell
778 heparan sulfate. Nat. Med. **3:**866-871.

779 50. **Chen, W., N. Gao, J. L. Wang, Y. P. Tian, Z. T. Chen, and J. An.** 2008. Vimentin is required
780 for dengue virus serotype 2 infection but microtubules are not necessary for this process.
781 Arch. Virol. **153:**1777-1781. doi: 10.1007/s00705-008-0183-x [doi].

782 51. **Phua, D. C., P. O. Humbert, and W. Hunziker.** 2009. Vimentin regulates scribble activity
783 by protecting it from proteasomal degradation. Mol. Biol. Cell. **20:**2841-2855. doi:
784 10.1091/mbc.E08-02-0199 [doi].

785 52. **van der Linden, L., K. C. Wolthers, and F. J. van Kuppeveld.** 2015. Replication and
786 Inhibitors of Enteroviruses and Parechoviruses. Viruses. **7:**4529-4562. doi:
787 10.3390/v7082832 [doi].

788 53. **Suhy, D. A., T. H. Giddings Jr, and K. Kirkegaard.** 2000. Remodeling the endoplasmic
789 reticulum by poliovirus infection and by individual viral proteins: an autophagy-like origin for
790 virus-induced vesicles. J. Virol. **74:**8953-8965.

791 54. **Limpens, R. W., H. M. van der Schaar, D. Kumar, A. J. Koster, E. J. Snijder, F. J. van**
792 **Kuppeveld, and M. Barcena.** 2011. The transformation of enterovirus replication structures:
793 a three-dimensional study of single- and double-membrane compartments. MBio.
794 **2:**10.1128/mBio.00166-11. Print 2011. doi: 10.1128/mBio.00166-11 [doi].

795 55. **Belov, G. A., V. Nair, B. T. Hansen, F. H. Hoyt, E. R. Fischer, and E. Ehrenfeld.** 2012.
796 Complex dynamic development of poliovirus membranous replication complexes. J. Virol.
797 **86:**302-312. doi: 10.1128/JVI.05937-11 [doi].

798 56. **Mogensen, T. H.** 2009. Pathogen recognition and inflammatory signaling in innate
799 immune defenses. Clin. Microbiol. Rev. **22:**240-73, Table of Contents. doi:
800 10.1128/CMR.00046-08 [doi].

801 57. **Toyoda, H., M. J. Nicklin, M. G. Murray, C. W. Anderson, J. J. Dunn, F. W. Studier, and**
802 **E. Wimmer.** 1986. A second virus-encoded proteinase involved in proteolytic processing of
803 poliovirus polyprotein. Cell. **45:**761-770. doi: 0092-8674(86)90790-7 [pii].

804 58. **Palmenberg, A. C.** 1990. Proteolytic processing of picornaviral polyprotein. Annu. Rev.
805 Microbiol. **44:**603-623. doi: 10.1146/annurev.mi.44.100190.003131 [doi].

806 59. **Firth, A. E., and I. Brierley.** 2012. Non-canonical translation in RNA viruses. J. Gen. Virol.
807 **93:**1385-1409. doi: 10.1099/vir.0.042499-0 [doi].

808 60. **Napthine, S., R. Ling, L. K. Finch, J. D. Jones, S. Bell, I. Brierley, and A. E. Firth.** 2017.
809 Protein-directed ribosomal frameshifting temporally regulates gene expression. Nat.
810 Commun. **8:**15582. doi: 10.1038/ncomms15582 [doi].

811 61. **Dinman, J. D.** 2012. Mechanisms and implications of programmed translational
812 frameshifting. Wiley Interdiscip. Rev. RNA. **3:**661-673. doi: 10.1002/wrna.1126 [doi].

813 62. **Donnelly, M. L., G. Luke, A. Mehrotra, X. Li, L. E. Hughes, D. Gani, and M. D. Ryan.**
814 2001. Analysis of the aphthovirus 2A/2B polyprotein 'cleavage' mechanism indicates not a
815 proteolytic reaction, but a novel translational effect: a putative ribosomal 'skip'. J. Gen.
816 Virol. **82:**1013-1025. doi: 10.1099/0022-1317-82-5-1013 [doi].

817 63. **Loughran, G., A. E. Firth, and J. F. Atkins.** 2011. Ribosomal frameshifting into an
818 overlapping gene in the 2B-encoding region of the cardiovirus genome. Proc. Natl. Acad. Sci.
819 U. S. A. **108:**E1111-9. doi: 10.1073/pnas.1102932108 [doi].

820 64. **Huang, S. Y., C. H. Huang, C. J. Chen, T. W. Chen, C. Y. Lin, Y. T. Lin, S. M. Kuo, C. G.**
821 **Huang, L. A. Lee, Y. H. Chen, M. F. Chen, R. L. Kuo, and S. R. Shih.** 2019. Novel Role for miR-
822 1290 in Host Species Specificity of Influenza A Virus. Mol. Ther. Nucleic Acids. **17:**10-23. doi:
823 S2162-2531(19)30121-0 [pii].

824 65. **Lawson, M. A., and B. L. Semler.** 1992. Alternate poliovirus nonstructural protein
825 processing cascades generated by primary sites of 3C proteinase cleavage. Virology.
826 **191:**309-320.

827 66. **Marjomaki, V., V. Pietiainen, H. Matilainen, P. Upla, J. Ivaska, L. Nissinen, H.**
828 **Reunanen, P. Huttunen, T. Hyypia, and J. Heino.** 2002. Internalization of echovirus 1 in
829 caveolae. J. Virol. **76:**1856-1865.

830 67. **Laitinen, O. H., E. Svedin, S. Kapell, M. M. Hankaniemi, P. G. Larsson, E. Domsgen, V.**
831 **M. Stone, J. A. E. Maatta, H. Hyoty, V. P. Hytonen, and M. Flodstrom-Tullberg.** 2018. New
832 Coxsackievirus 2A(pro) and 3C(pro) protease antibodies for virus detection and discovery of
833 pathogenic mechanisms. J. Virol. Methods. **255:**29-37. doi: S0166-0934(17)30716-4 [pii].

834 68. **Nuanualsuwan, S., and D. O. Cliver.** 2003. Capsid functions of inactivated human
835 picornaviruses and feline calicivirus. Appl. Environ. Microbiol. **69:**350-357.

836 69. **Nuanualsuwan, S., and D. O. Cliver.** 2003. Infectivity of RNA from inactivated poliovirus.
837 Appl. Environ. Microbiol. **69:**1629-1632.

838 70. **Kankaanpaa, P., L. Paavolainen, S. Tiitta, M. Karjalainen, J. Paivarinne, J. Nieminen, V.**
839 **Marjomaki, J. Heino, and D. J. White.** 2012. BioImageXD: an open, general-purpose and
840 high-throughput image-processing platform. Nat. Methods. **9:**683-689. doi:
841 10.1038/nmeth.2047; 10.1038/nmeth.2047.

842

843

844 **FIGURE LEGENDS**

845

846 **Fig 1. Human enterovirus infection induces vimentin enwrapped dsRNA-harboring**
847 **compartment to the perinuclear location in A549 cells.** A549 cells were fixed,
848 immunolabeled, and visualized with confocal microscopy. (A) Images from single sections
849 showing vimentin (green) and virus capsid (magenta) in cells after CVB3 (5 h p.i.) infection.
850 (B) Vimentin (green) and tubulin (magenta) network in non-infected (ctrl) and CVB3 infected
851 (5 h p.i.) cells. Infected cells are marked with asterisk. (C) Images from single sections
852 showing vimentin (green) and virus capsid (magenta) in cells after EV1 (6 h p.i.), CVB1 (6 h
853 p.i.), and CVA9 (5h p.i.) infections. Non-infected cells are marked with asterisks. (D)
854 Projection of Z-sections showing dsRNA (green) and vimentin (Magenta). Orthogonal
855 sections providing a view of these structures in 3D after CVB3 infection (5 h p.i.). (E) Images
856 of single sections showing vimentin structure formation from 2.5 h to 6h p.i. Cell boundaries
857 drawn to visualize state of cell detachment.

858 **Fig 2. The appearance of VP1 and dsRNA coincide with vimentin rearrangements during**
859 **CVB3 infection.** A549 cells were fixed, immunolabeled, and visualized with confocal
860 microscopy. (A) Single section images showing vimentin and VP1 (capsid) at different
861 timepoints p.i. (B) Quantifications of confocal images taken at different time points during
862 CVB3 infection. The results shown here are representations of at least three independent
863 experiments. For the quantifications, approximately 200 cells altogether from two to three
864 replicates were analyzed (+/-SEM). Scale bars 20µm

865 **Fig 3. Viral protein synthesis is essential for the vimentin cage formation.** (A) Schematic
866 illustration showing the principle of neutral red viruses (top). A549 cells infected with
867 neutral red-CVB3 exposed to light treatment at different time points, and the presence of

virus-induced vimentin structures was visualized from single section confocal images and quantitated. For the quantifications, approximately 50 cells per sample of three replicates were analyzed. (B) Single section confocal images illustrating the effect of UV-inactivated EV1 on A549 cells at 6 h p.i.. Cells were immunolabeled for capsid (green) and vimentin (magenta) (C) Graphs showing the results of the CPE experiment in CVB3-infected A549 after differential treatments with either cycloheximide (200 µg/ml) or puromycin (100 µg/ml). Drugs were added to the cells at different time points p.i. and left until the end of the experiment (8h p.i.). Control cells were normalized to 100 %. Representative of at least two separate experiments with three replicate samples within each. (D) Single section confocal images visualizing vimentin (green) and virus capsids (red) in CVB3-infected (5 h p.i.) A549 cells with ctrl, puromycin (100 µg/ml) or cycloheximide (200 µg/ml) treatment when the drugs were introduced at 2 h p.i. Scale bars 20 µm. Representative of at least two separate experiments. (E) Western blot showing VP1 expression in infected cells after cycloheximide (200 µg/ml) or puromycin (100 µg/ml) treatments. The drugs were added at 2 h p.i. and left until the end of the experiment (5.5 h p.i.). Representative of at least two separate experiments. (F) RT-qPCR from CVB3 infected cells treated with or without cycloheximide (200 µg/ml) or puromycin (100 µg/ml). Virus (8.86 x 10^7 PFU/ml) was bound on cells on ice for 1 h. After washing excess virus, the infection was allowed to proceed for 5.5 h. The drugs were added at 2 h p.i. and left until the end of the experiment. N/A, signal is below detection threshold. (G) Graph showing the results of the cell viability measurement (ATP) of CVB3-infected A549 after differential treatments with either VER155008 (50 µM) or geldanamycin (0.1 µM). Drugs were added to the cells together with the virus and left until the end of the experiment (10 h.). Representative of at least two separate experiments with three replicate samples within each. (H) The quantification of confocal images of CVB3-infected, VER155008 and Geldanamycin treated A549 cells

showing virus-induced vimentin structures. Data was obtained from at least 100 cells from two independent experiments. (I) Single section confocal images showing dsRNA (green) in CVB3 infected cells with or without VER155008 (50 µM) or geldanamycin (0.1 µM) treatments. Virus (4.43 x 10^8 PFU/ml) was bound on ice for 1 h, and after washing excess virus, the infection was allowed to proceed for 5.5 h. The drugs were added after ice binding and left until the end of the experiment. Scale bars 20 µm. (J) Western blot showing VP1 expression in infected cells after VER155008 (50 µM) or geldanamycin (0.1 µM) treatments. The drugs were added to the cells together with the virus and left until the end of the experiment (5.5 h p.i.). Representative of at least two separate experiments.

Fig 4. IDPN treatment delays virus-induced cell death without compromising the production of progeny viruses. (A) Graph showing the effect of IDPN treatment on A549 cell viability. Representative of two replicates. (B) Single section images showing vimentin distribution after 5.5 h of 1.5% IDPN treatment. Representative of at least three separate experiments. (C) Graph showing cell viability (ATP) in CVB3 infected A549 cells with and without IDPN treatment (1.5 %). Drug was added together with the virus and kept until the end of the experiment. Representative of at least two separate experiments with three replicate samples within each. (D) End-point titration of progeny viruses produced after 6 h CVB3 infection in A549 cells with or without IDPN treatment. Representative of two independent experiments. (E) RT-qPCR from cells infected with CVB3 for 1, 3, 4 or 5 h with or without IDPN treatment. Virus (8.86 x 10^7 PFU/ml) was bound on cells on ice for 1 h. After washing excess virus, the infection was allowed to proceed for the indicated time. IDPN was added after ice binding and left until the end of the experiment. (F) Single section confocal images illustrating the effect of IDPN on replication (dsRNA, green) and vimentin (magenta). Representative image of at least three replicates. Scale bar 20 µm.

Fig 5. Vimentin cage preferentially hosts non-structural proteins. (A) Single sections showing location of 3D magenta or (B) 2A (magenta) in the perinuclear area and vimentin (green) in control or CVB3 infected cells with or without IDPN treatment. Virus (4.43 x 10^8 PFU/ml) was bound on ice for 1 h. After washing the excess virus away, infection was allowed to proceed for 5.5 h. IDPN was added after ice binding and left until the end of the experiment. (C) Single sections showing the location of VP1 diffusely in the cytoplasm in CVB3 infected cells with or without IDPN treatment. Infection was carried out as described above in B. Scale bars 20 µm. Representative images of at least three separate experiments. (D) Single section confocal images illustrating the effect of IDPN on (D) ER (PDI) (5.5. h p.i) and (E) Golgi (GM130) (5.5 h p.i). Scale bar 20 µm. The images are representative of at least two separate experiments.

Fig 6. Inhibition of vimentin dynamics affects the levels and activity of non-structural proteins. (A) Graphs showing quantifications of western blots where levels of VP1, 2A, 3C and 3D were detected in CVB3 infected A549 cells with or without IDPN treatment. Virus (4.43 x 10^8 PFU/ml) was bound on ice for 1 h. After washing the excess virus away, infection was allowed to proceed for 5.5 h. IDPN was added after ice binding and left until the end of the experiment. Band intensities were quantified using Image J and the quantifications were done from at least three separate experiments. (B) Western blots were immunolabeled with antibodies against PABP, G3BP1, VP1 and GAPDH. Arrowhead indicates CVB3 induced cleavage product. Representative of at least two separate experiments. (C) Graphs showing the results of the viability measurement (C) and caspase activity (D) per viable cell of A549 cells treated with z-vad fmk (200µM) or IDPN (1.5%) with or without CVB3 infection. Drugs were added to the cells together with the virus and left until the end of the experiment (10 and 24 h p.i.). Graphs are showing the results from three independent experiment. (E)

941 Western blots were immunolabeled with antibodies against eIF4G, VP1 and GAPDH.
942 Representative of at least two separate experiments. (F) Pulse labeling of CVB3 infected
943 cells with or without 1.5% IDPN treatment. Virus (4.43 x 10^8 PFU/ml) was bound on ice for
944 1h after which the excess virus was washed away. IDPN was added after ice binding and left
945 until the end of the experiment. Pulse labeling with radioactive Sulphur (500 µCi/ml) was
946 carried out at 4.5-5.5 h p.i. Representative of two separate experiments. (G)
947 Immunoblotting performed after SDS-PAGE showing the expression status of different ER
948 markers with and without CVB3 (5.5 h p.i.) and/or IDPN in A549 cells. Tunicamycin (TM;
949 5µg/ml) was used as a positive control and GAPDH as a loading control. (H) Luminescence
950 measurement indicating the ROS activation in A549 cells without CVB3 (6 h p.i.) and/or
951 IDPN. Graphs are showing the results from three independent experiment. (* = P <0.05).

952 **Fig 7**. **Vimentin dynamics affect the synthesis of non-structural proteins rather than their**
953 **degradation.** (A) Western blot of A549 cells infected with CVB3 for 3, 4, 5 or 6 h with or
954 without IDPN treatment. Virus (4.43 x 10^8 PFU/ml) was bound on ice for 1h. After washing
955 the excess virus away, infection was allowed to proceed for the indicated time. IDPN was
956 added after ice binding and left until the end of the experiment. eIF4G, 3D, 2A and VP1
957 were visualized using antibodies against the proteins. Representative image of two
958 replicates. (B) Western blot showing the effect of 1.5% IDPN, 7 µM bortezomib, 200 µM
959 Calpain inhibitor 1, 100 µg/ml puromycin, 50 µM VER155008 or 0.1 µM geldanamycin on
960 CVB3 infection. Virus (4.43 x 10^8 PFU/ml) was bound on ice for 1 h. After washing the excess
961 virus away, infection was allowed to proceed for 5.5 h. Other drugs were added after ice
962 binding except calpain inhibitor, bortezomib and puromycin, which were added at 2 h p.i. All
963 drugs were left until the end of the experiment. Visualization of VP1 and P1 on the left.

964 Merged image of 2A and VP1 labelings on the right. Representative results of at least two
965 separate experiments.

966 **Fig 8. Summary.** Viral protein synthesis during enterovirus infection induces formation of a
967 vimentin enwrapped perinuclear compartment harboring the viral non-structural proteins.
968 Inhibition of vimentin rearrangements leads to scattered distribution of non-structural
969 proteins and their lower expression and activity, without affecting the structural proteins
970 and viral progeny production. Stars indicate the magnitude of the phenomenon. NS-
971 proteins, non-structural proteins.

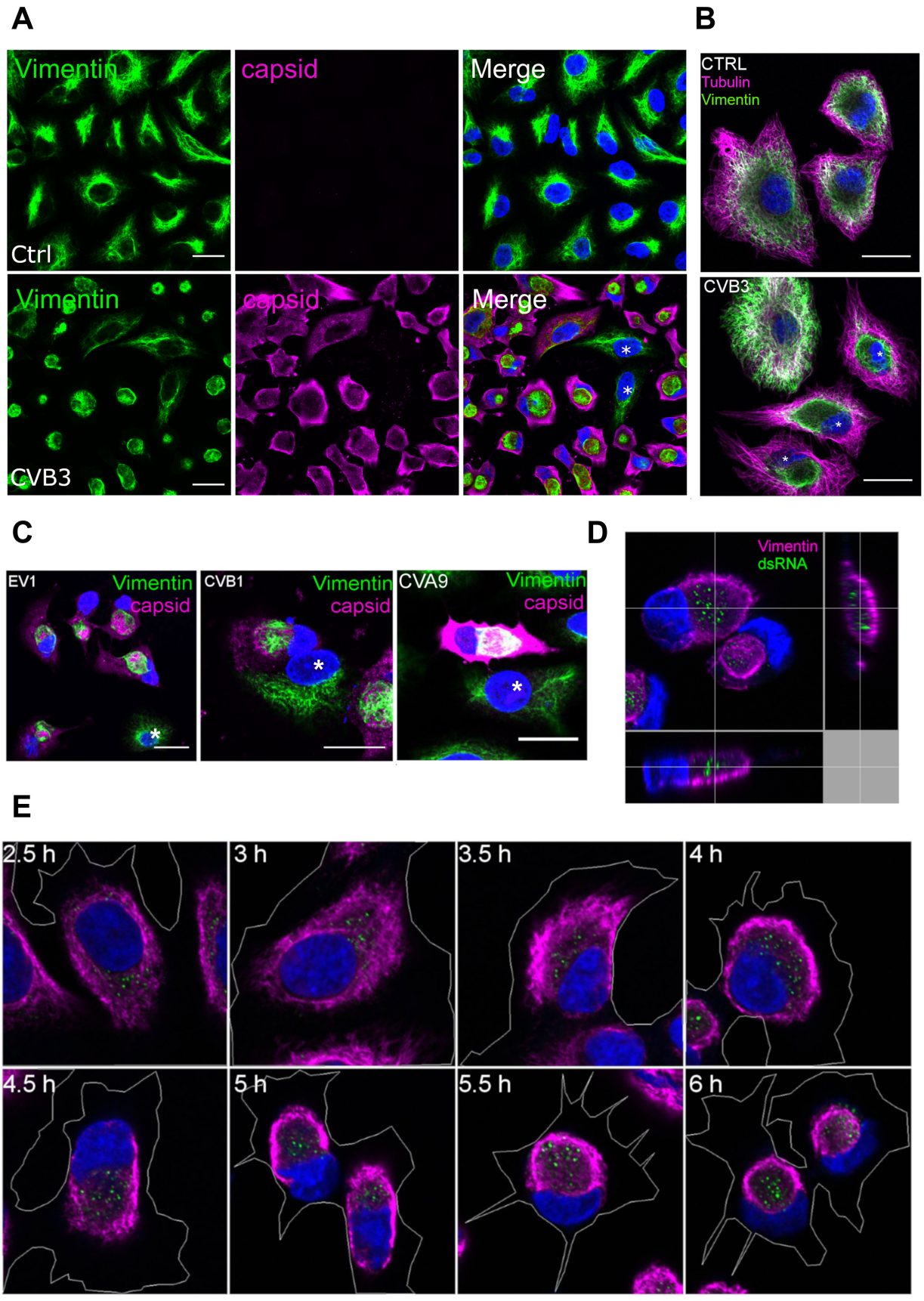

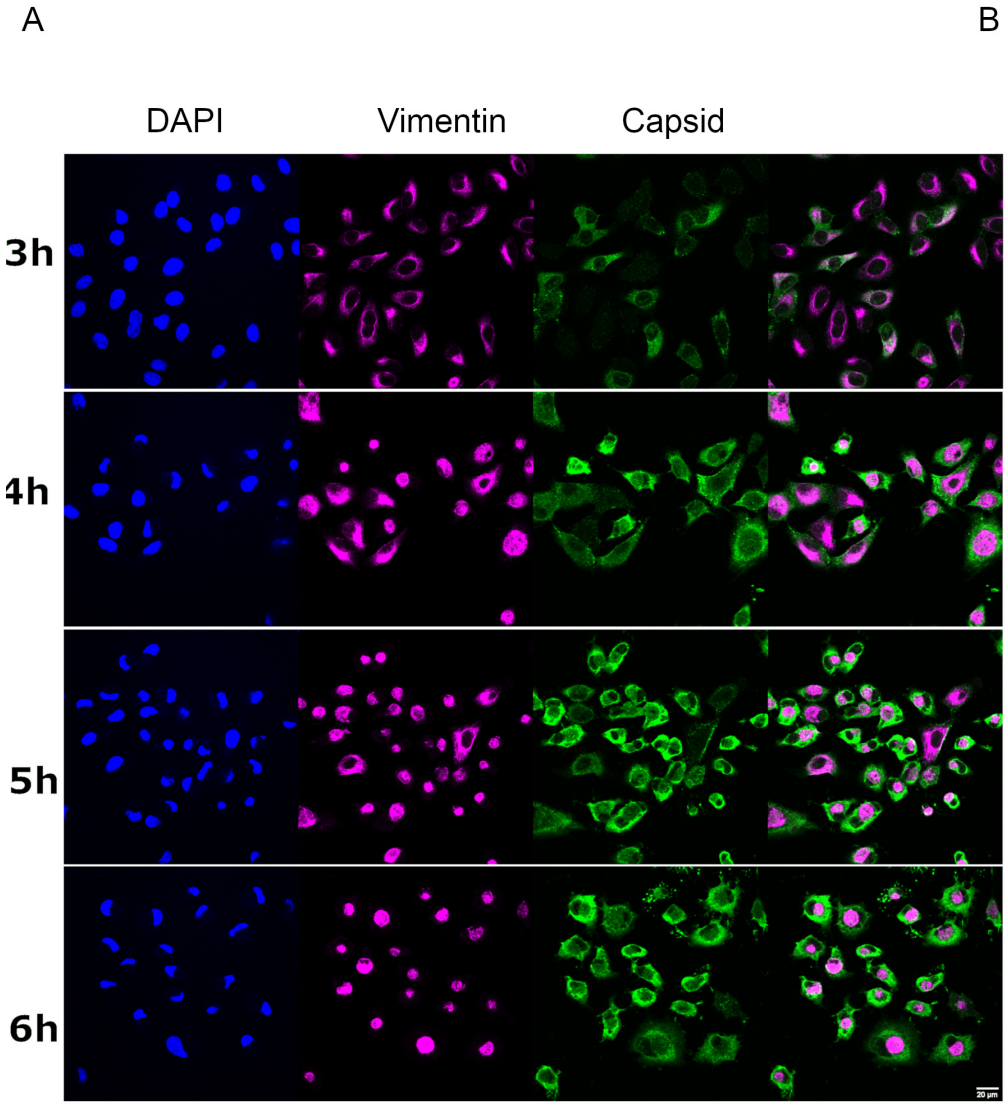

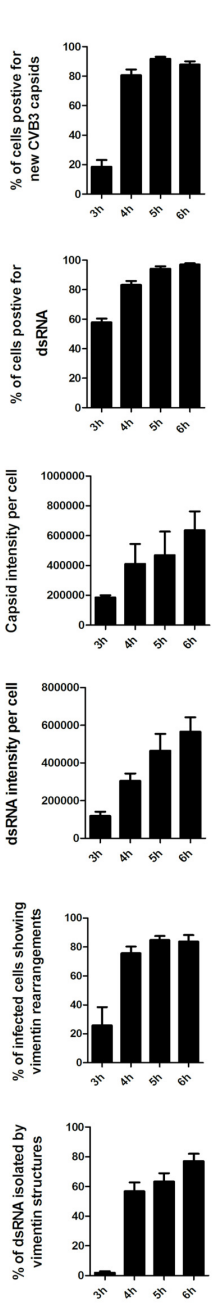

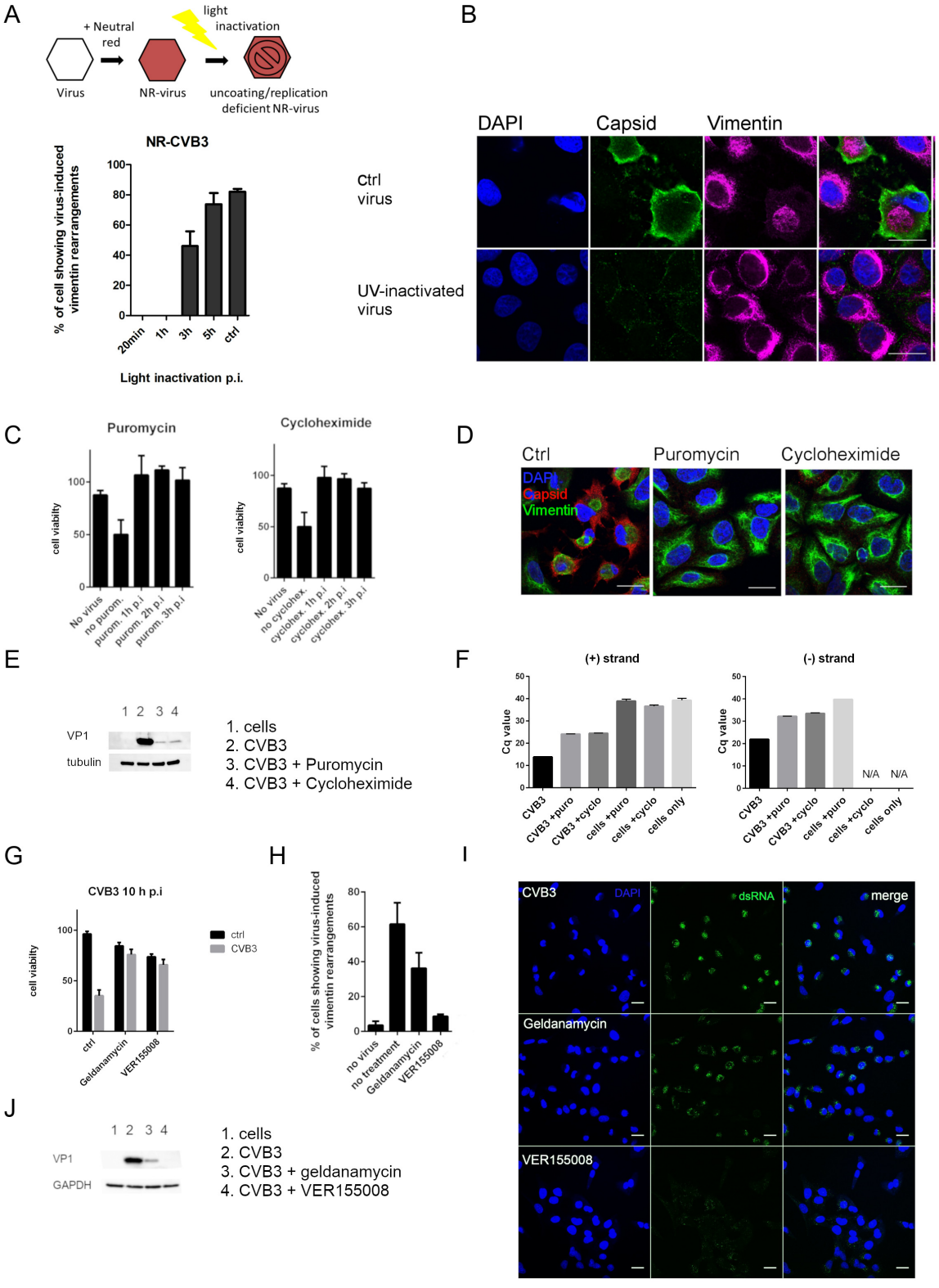

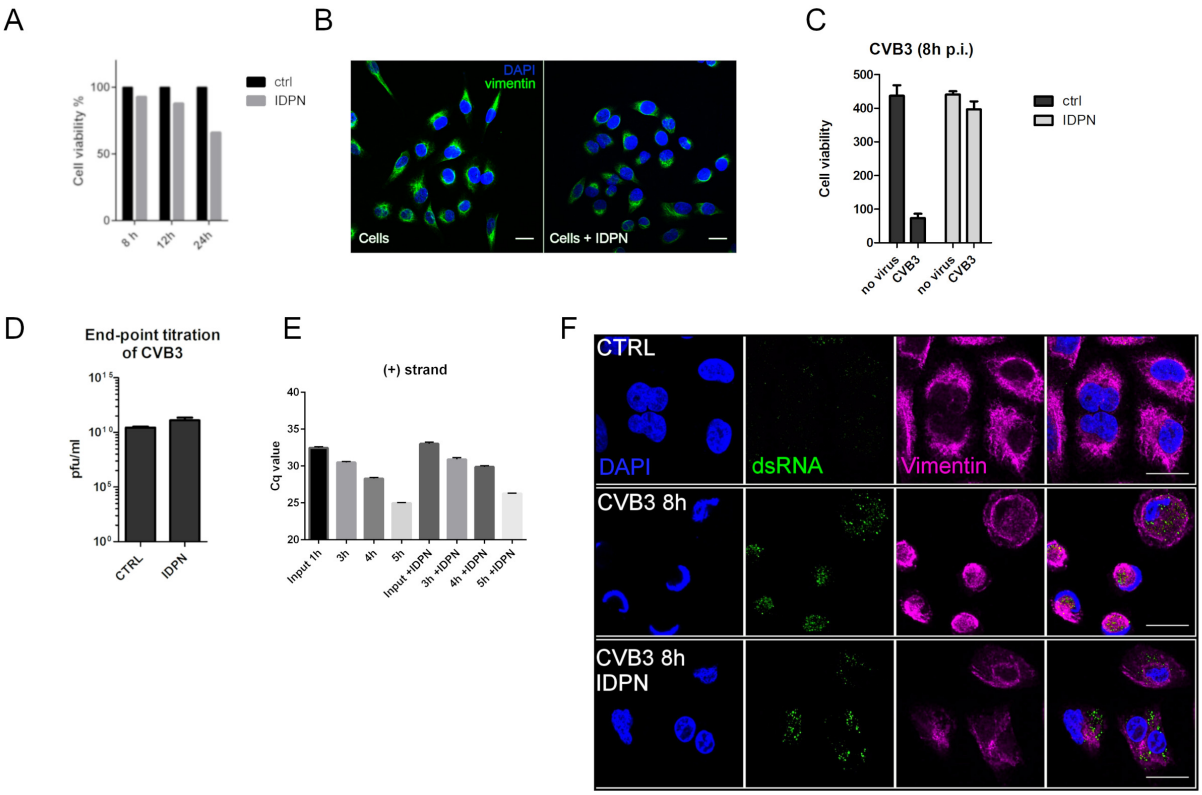

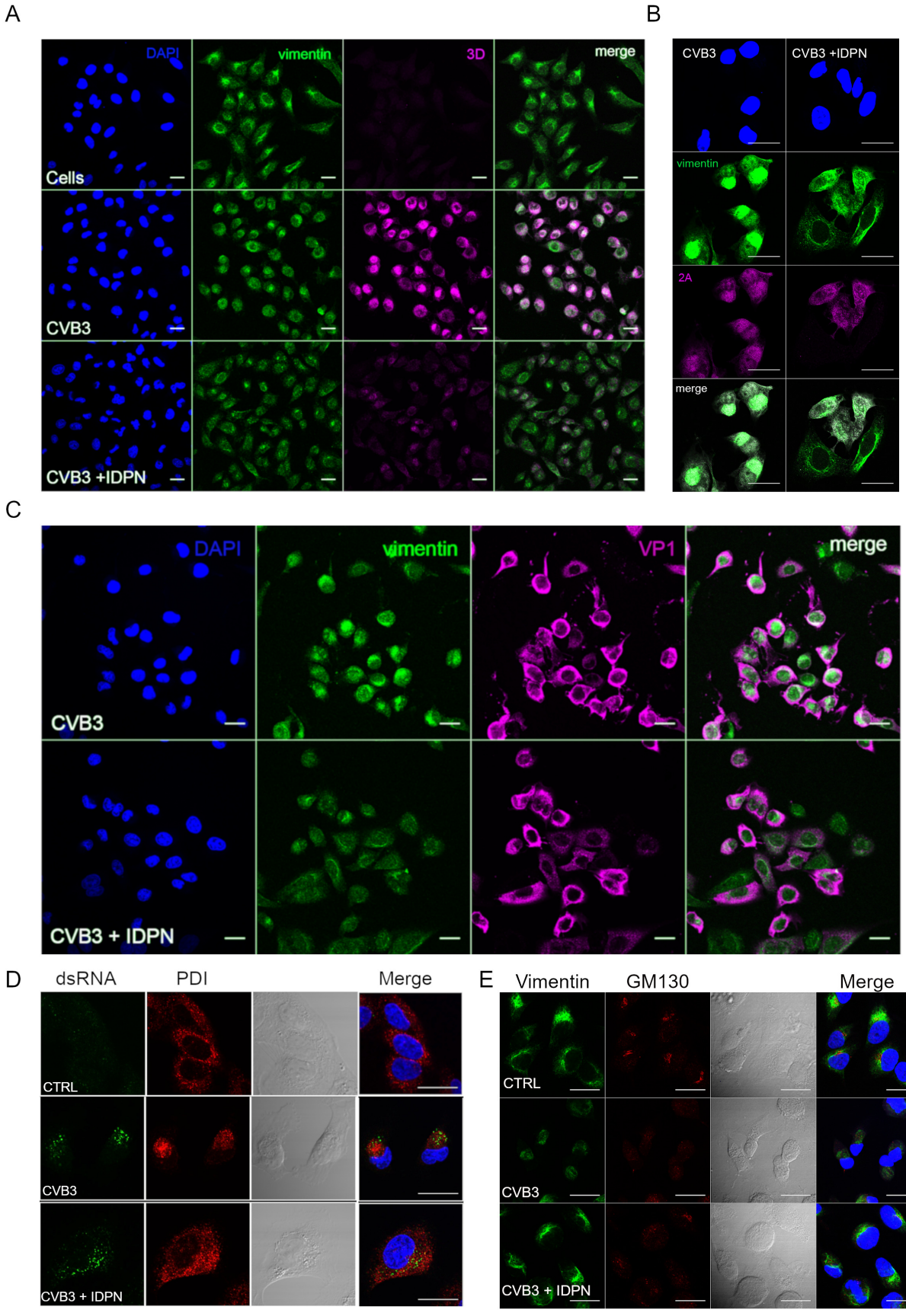

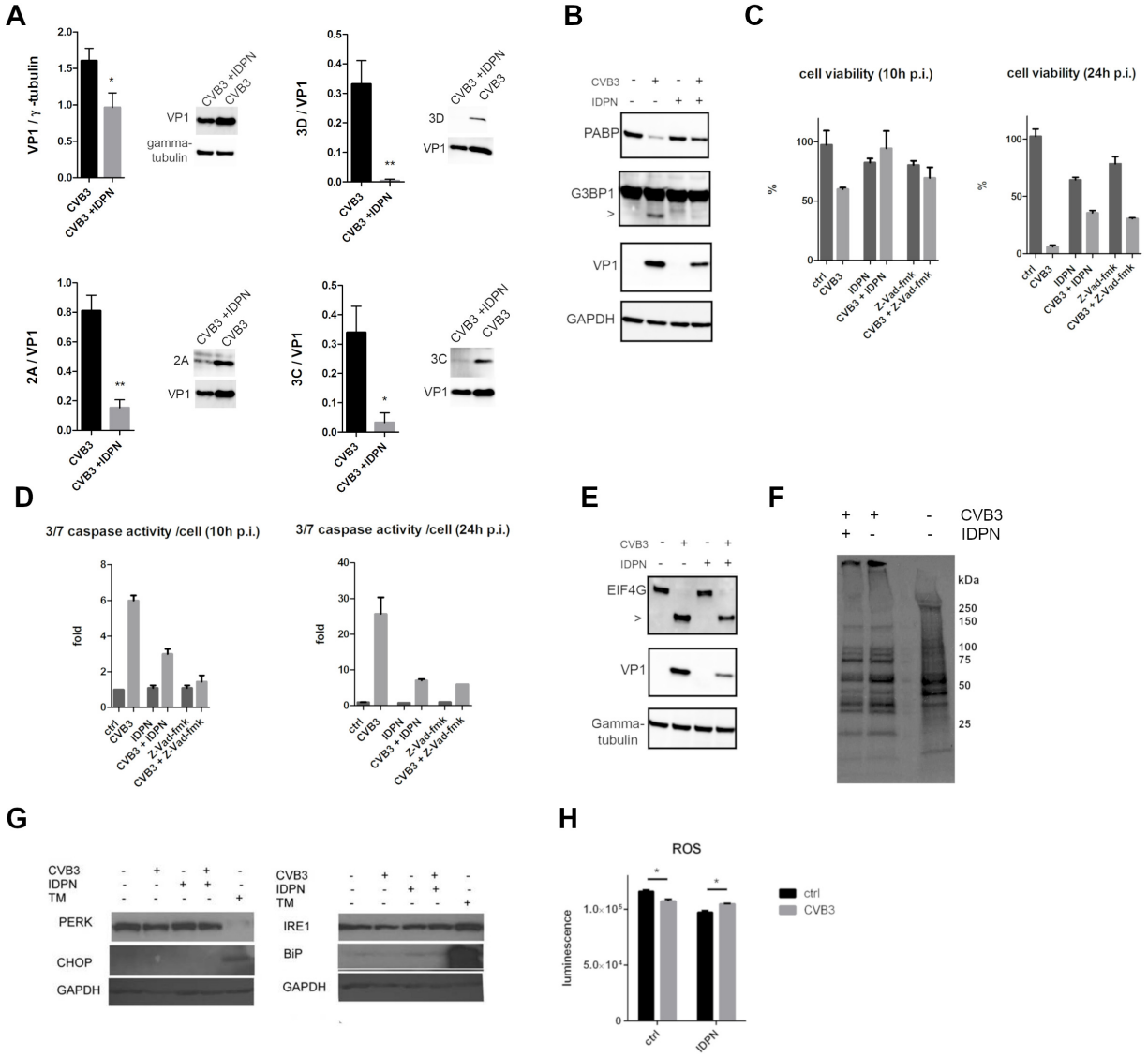

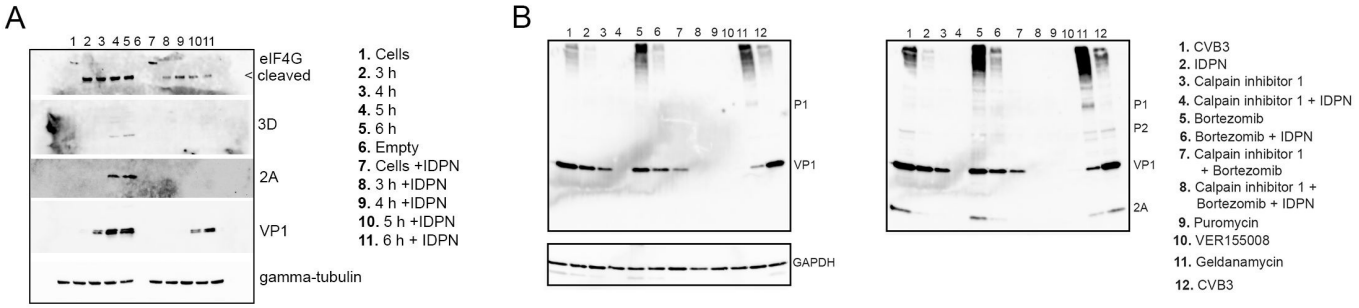

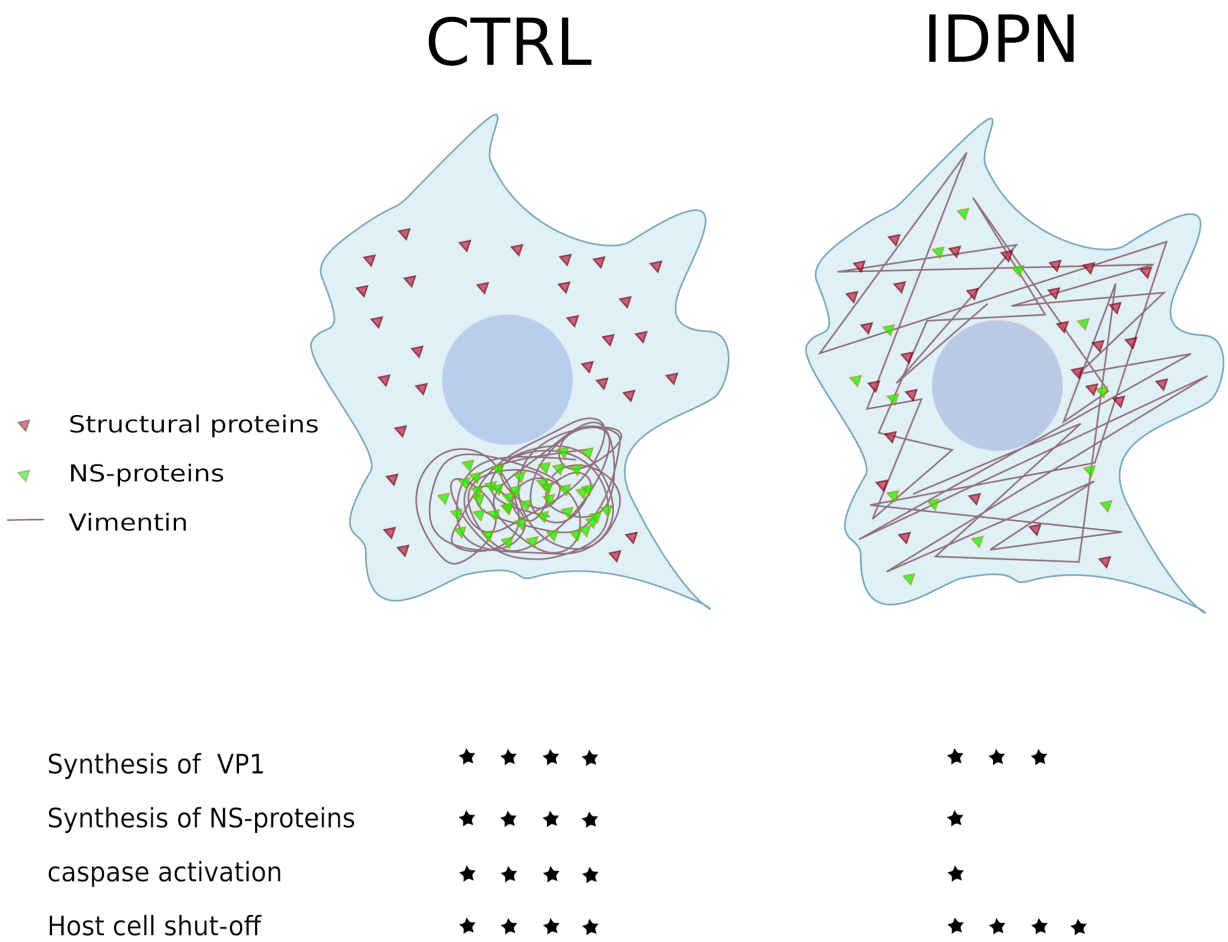

	CTRL	IDPN
Synthesis of VP1	★ ★ ★ ★	★ ★ ★
Synthesis of NS-proteins	★ ★ ★ ★	★
caspase activation	★ ★ ★ ★	★
Host cell shut-off	★ ★ ★ ★	★ ★ ★ ★

Structural proteins
processed mainly in the soluble pool
processing dependent on Hsp90

Non structural proteins
processing associated with vimentin cages

Journal of Virology
JVI
Journal of Virology